ISPRS Journal of Photogrammetry and Remote Sensing 167 (2020) 432–442

Contents lists available at ScienceDirect

ISPRS Journal of Photogrammetry and Remote Sensing

journal homepage: www.elsevier.com/locate/isprsjprs

Structure-aware Building Mesh Polygonization

Vasileios Bouzas, Hugo Ledoux, Liangliang Nan *

3D Geoinformation Research Group, Faculty of Architecture and the Built Environment, Delft University of Technology, 2628 BL Delft, The Netherlands

ARTICLE INFO

Keywords:
MVS meshes
Structure awareness
Polygonization
Simplification

ABSTRACT

We introduce a novel approach for the polygonization of Multi-view Stereo (MVS) meshes of buildings, which results in compact and topologically valid models. The main characteristic of our method is *structure awareness*, i.e., the recovery and preservation of the initial mesh primitives and their adjacencies. Our proposed methodology consists of three main stages: (a) primitive detection via mesh segmentation, (b) encoding of primitive adjacencies into a graph, and (c) polygonization. Polygonization is based on the approximation of the original mesh with a candidate set of planar polygonal faces. On this candidate set, we apply a binary labelling formulation to select and assemble an optimal set of faces under hard constraints that ensure that the final model is both manifold and watertight. Experiments on various building models demonstrate that our simplification method can produce simpler representations for both closed and open building meshes. Furthermore, these representations highly conform to the initial structure and are ready to be used for spatial analysis. The source code of this work is freely available at https://github.com/VasileiosBouzas/MeshPolygonization.

1. Introduction

In recent decades, there is an ever-increasing demand, both by academia and industry, for 3D spatial information and 3D City models (Biljecki et al., 2015). In contrast to 2D data, 3D data either provides a much more enriched context for some applications or makes others possible. Applications that benefit from the use of 3D data vary from infrastructure planning, utility management, and 3D cadastre to solar potential estimation and visibility analysis.

One common practice to obtain 3D models of buildings and urban scenes is the acquisition of massive point clouds through Airborne Laser Scanning (ALS), Structure from Motion (SfM), or Multi-view Stereo (MVS) (Furukawa and Hernández, 2015). These point clouds, combined with reconstruction techniques (Bernardini et al., 1999; Kazhdan et al., 2006), enable the representation of buildings in the form of *surface meshes*. Although the quality of these meshes is sufficient for visualization purposes, it is still not enough for other applications, such as urban planning and simulations (Holzmann et al., 2017), due to:

- *Large memory size*: The number of faces also increases the requirements of these meshes in memory space.
- *Missing information*: The incompleteness of the original point cloud, due to occlusion or other causes, often prevents the reconstruction of a given scene in its entirety.
- *Noisy and undesired structures*: Flaws both in the original point cloud and the reconstruction method lead to defects in the final mesh (e.g., self-intersecting parts or holes).

These problems are often addressed with mesh *simplification* and *polygonization*. Despite the similarities of these two approaches, *simplification* relates to the removal of redundant faces for representing the original mesh (Garland and Heckbert, 1997). On the other hand, the objective of *polygonization* is the approximation of the original mesh with a set of polygonal surfaces. The existing simplification and polygonization techniques (Garland and Heckbert, 1997; Salinas et al., 2015; Cohen-Steiner et al., 2004) succeed in the production of lightweight meshes with less complexity and memory requirements than their original counterparts. However, these meshes often lack the topological validity necessary for their use in real-world applications such as simulations.

In this work, we propose a novel approach for producing *simpler, more compact* representations for MVS building meshes through *polygonization* (see Fig. 1). Our inputs are building mesh models acquired from aerial and terrestrial imagery, for which we assume that the building instances are extracted from urban scenes via semantic segmentation (Landrieu and Simonovsky, 2018; Verdie et al., 2015; Rouhani et al., 2017; Zhu et al., 2018; Valentin et al., 2013). Also, we mainly target buildings whose geometry can be represented by closed

* Corresponding author.
E-mail addresses: bouzasbasilis@gmail.com (V. Bouzas), h.ledoux@tudelft.nl (H. Ledoux), liangliang.nan@gmail.com (L. Nan).

https://doi.org/10.1016/j.isprsjprs.2020.07.010
Received 6 March 2020; Received in revised form 16 July 2020; Accepted 20 July 2020

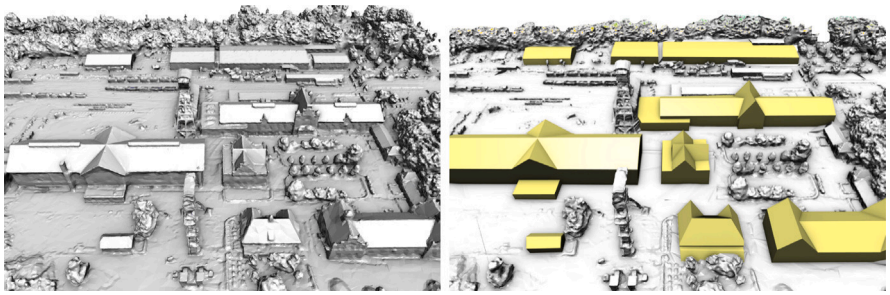

Fig. 1. An urban scene with it buildings simplified using our method. Each building was simplified individually after the semantic segmentation of the scene).

polyhedra without dangling faces. We assess the effectiveness of our simplification method with several criteria. Apart from a lightweight representation of the original model, the resulting mesh should be also *manifold*, *watertight*, and free of geometric errors. This allows us to use it as input in software for different applications (e.g., energy estimation, wind simulation, cadastre, and solar potential). Furthermore, the outcome of this method should be independent of any imperfections in the original mesh (e.g., geometric or topological defects, noise, and undesired structures). Finally, simplification results should be accomplished within reasonable execution times to allow the processing of large scale environments.

To achieve polygonization, we first detect the planar components (*geometry*) of the input mesh along with their configuration (*topology*) in the 3D space. Based on this information, we form an initial set of *candidate faces* to approximate the mesh. To construct the simplified model, we select candidate faces through a constrained optimization process that ensures the final result is both manifold and watertight. Our contributions to the current state of the art are the following:

- A novel *mesh segmentation* technique based on region growing for the detection of planar components in surface meshes;
- An optimization-based method for the construction of the simplified surface models based on the definition of *sharp features* through a *building scaffold* and of *faces* through *2D arrangements*.

2. Related work

There is a large volume of research on mesh polygonization. In this section, we only review the most relevant work in the scientific literature for topics directly related to ours.

Planar shape detection/abstraction. Contrary to natural objects, man-made constructions conform to clearly defined geometries, thus allowing their approximation via an assembly of planar shapes. This approximation stands as the basis for several mesh simplification/polygonization techniques and therefore, there has been an extensive literature on the detection and abstraction of planar shapes both in point clouds and meshes. Several approaches to this problem (region growing/RANSAC (Schnabel et al., 2007)) attempt to decompose the input cloud or mesh into planes in one go, based on one or more attributes (normal orientation, curvature, planarity, etc.). Others use this decomposition as input for an optimization process during which the initial planar set needs to conform to a predefined metric (Monszpart et al., 2015; Oesau et al., 2015; Fang et al., 2018; Jonsson, 2016). Following these work, we contribute to the current state of the art with our proposed mesh segmentation technique (see Section 3.1).

Plane assemblies. The detection and assembly of planar shapes for the construction of compact polygon meshes constitute the core of our method. As in other existing methods (Nan and Wonka, 2017; Chauve et al., 2010; Chen and Chen, 2007; Bauchet, 2019; Fang, 2019), the main problems to be addressed in this approach is the completeness of the final result despite imperfections in the input data (geometric/topological flaws, holes, and noise, etc.). While a holistic approach (i.e. pairwise intersections between all available planes) proves to be enough for tackling this problem, it often increases execution time considerably. To balance this trade-off between completeness and computational efficiency, it is therefore necessary to reduce the number of computations but not at the expense of the quality of the result. In our method, this is achieved with the introduction of our structure graph.

Urban reconstruction. The various methods currently existing for the reconstruction of urban environments are divided into three main categories: (1) *building mesh reconstruction* (Holzmann et al., 2017; Nan and Wonka, 2017; Li et al., 2016; Bódis-Szomorú et al., 2015), (2) *building mesh regularization* (Jonsson, 2016; Wang et al., 2016; Kelly et al., 2017), and (3) *urban scene reconstruction* (Verdie et al., 2015; Zhu et al., 2018). The first two categories produce 3D models for individual buildings, while the third one focuses on recreating entire urban scenes. Despite their effectiveness, many of these methods depend on multiple sources of information that are not always available (e.g., aerial imagery, point clouds, GIS data) (Kelly et al., 2017; Zhu et al., 2018). Others conform to the already reconstructed models to certain geometric regulations (e.g., vertex projection to planar primitives, orthogonality, perpendicularity), but still maintain the initial number of meshes faces (Bódis-Szomorú et al., 2015; Jonsson, 2016; Wang et al., 2016). Our method satisfies both the requirements of geometric regularity and simple representation, with only the reconstructed mesh as an input.

Mesh simplification/polygonization. In computer graphics, various methods exist for the simplification of 3D meshes, mainly for visualization and animation purposes. For example, Quadric Error metrics (QEM) (Garland and Heckbert, 1997) or Structure-Aware Mesh Decimation (SAMD) (Salinas et al., 2015) simplifies meshes by iteratively reducing the number of their simplexes. A characteristic example of polygonization techniques is Variational Shape Approximation (VSA) (Cohen-Steiner et al., 2004), which constructs an entirely new mesh that approximates the original model and consists of planar shapes (*proxies*). In either case, the topological validity of the simplified mesh, essential for its usage in further applications, is not always ensured. In this work, we combine simple representation with topological validity, resulting in building models ready for spatial analysis.

Structure awareness. Although the concept of *structure* still lacks any universally accepted definition, there has been some research on structure-aware shape processing over the last decades (Mitra et al., 2013; Salinas et al., 2015). Regardless of their unique characteristics, most structure-aware approaches define the structure of an object as the assembly of two elements: **(a)** the *parts* composing the object and **(b)** the *interrelationships* between these object parts. In return, shape processing also consists of two separate procedures: structure detection and processing according to the detected structure.

In this paper, we assume that the majority of real-world buildings demonstrate piecewise planar structures. We define the *structure* of a building by detecting the planar primitives of the input model along with their adjacency relations. Furthermore, any information on the structure is encoded into a *structure graph*, an undirected graph whose vertices correspond to the detected primitives while the edges denote adjacency relations between primitive pairs. The main advantages of structure awareness, in the form of the structure graph, for the simplification process are the following:

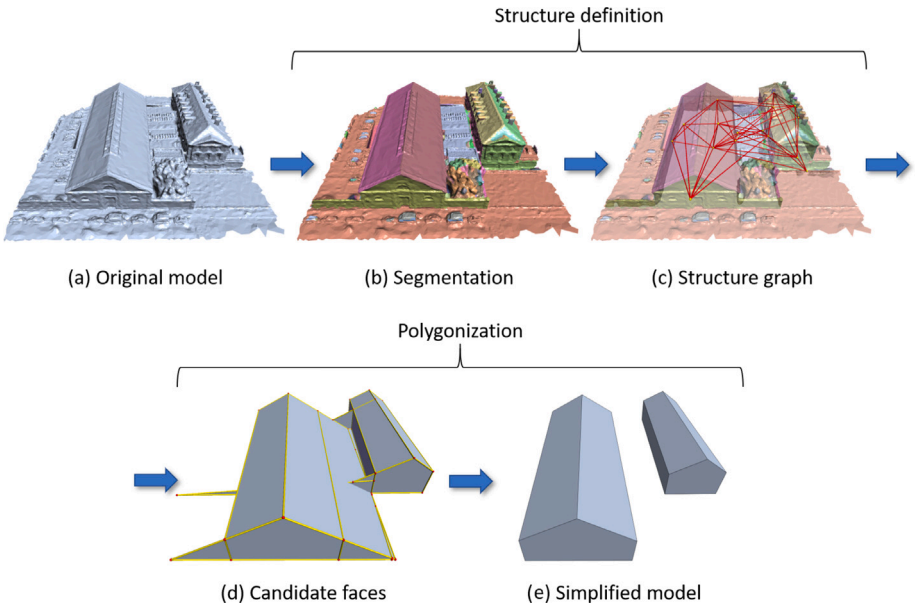

Fig. 2. Pipeline. The input MVS building mesh **(a)** is decomposed into planar primitives **(b)** and its structure is encoded into the structure graph **(c)**. With the help of the graph, a set of *candidate faces* is produced **(d)** out of which the simplified model is finally constructed via optimization **(e)**.

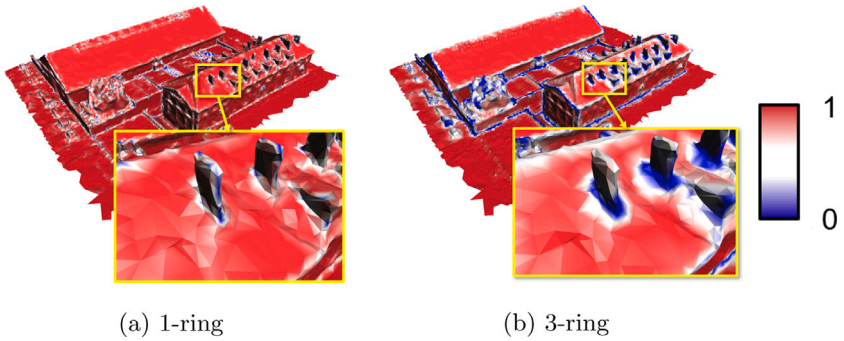

Fig. 3. Two examples of k-ring planarity for the vertices of a given mesh. Planar regions (high planarity) are coloured in red, while non-planar (low planarity) in blue. (For interpretation of the references to colour in this figure legend, the reader is referred to the web version of this article.)

- The structure of the original model is retained in the simplified version by preserving the formation of the graph along the simplification process.
- The *sharp features* of the original model, formed out of adjacent components, are recovered during polygonization by maintaining the adjacencies in the graph.

3. Methodology

As shown in Fig. 2, our methodology consists of three main processing stages: **(a)** detection of primitives via *segmentation*, **(b)** encoding of the primitive interrelationships in a *structure graph*, and **(c)** structure-aware *polygonization*.

3.1. Segmentation

To define the structure, we first identify the primitives of the input mesh via *segmentation*. We presume that the input mesh is composed only of planar components, thus ignoring any spherical, cylindrical, and conical geometries. The planar regions we wish to detect correspond to *floor*, *façade*, and *roof* segments, while any architectural details (e.g., windows, chimneys) are ignored. These details are usually represented by a small number of faces due to the limited resolution of MVS meshes, therefore their approximation with planar components is difficult (Verdie et al., 2015).

We detect planar segments via a *region-growing* algorithm, based on the computation of planarity for the k-ring neighbourhood of each mesh vertex (Gatzke and Grimm, 2006). Specifically, the 1-ring neighbourhood of a vertex consists of all vertices directly connected to it through an edge. This notion of a neighbourhood can be defined for extended mesh regions (for example, a 2-ring neighbourhood includes also the vertices adjacent to those forming the 1-ring neighbourhood), as well as for mesh faces. Hence, the k-ring planarity of a vertex describes the degree of fitting a plane on its k-ring neighbourhood (Pauly et al., 2002).

Our segmentation algorithm can be summarized as follows (for further details, see Algorithm 1):

(a) We compute the k-ring planarity of all the mesh vertices, while the planarity of each face is set equal to the *average* planarity of its vertices.
(b) With the highest planarity face (*seed*), we initialize the first planar region and collect its k-ring neighbours to define a *reference plane* via Principal Components Analysis (PCA) (Pauly et al., 2002).
(c) By examining the k-ring neighbourhoods of the seed, we append faces in the region as long as their vertices are within a *distance threshold* from the reference plane.
(d) We repeat the whole process till the entirety of the mesh has been decomposed into planar regions.

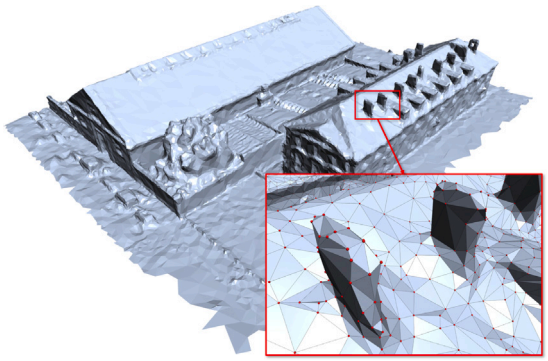

Fig. 4. In MVS meshes, architectural details (chimneys etc.) are represented by a small number of faces.

3.2. Structure graph

We detect interrelationships between the primitives of the segmentation and encode that information to an undirected graph (*structure graph*), resembling the *graph of proxies* of SAMD (Salinas et al., 2015). Each graph *vertex* corresponds to a primitive, while a pair of vertices is connected with an *edge* if their respective planar regions are adjacent. Our *structure graph* mainly serves two purposes:

- To determine the components of the simplified mesh along with their configuration in the 3D space, according to the structure of the original model. In this way, we guarantee that the result of our method closely approximates the initial model.
- To indicate only the pairwise intersections necessary for recovering edges of the simplified mesh, instead of computing all of them. As a consequence, computational complexity considerably decreases in comparison with traditional plane assembling methods such as Polyfit (Nan and Wonka, 2017).

Similar to other techniques, our segmentation method often identifies more planar segments than those present in the input mesh (*oversegmentation*). To address this problem, we apply a *refinement* process over the initial segmentation, similar to Nan and Wonka (2017). The refinement reduces the original number of planar segments by iteratively merging them into new ones. In particular, two segments are merged if they share the same orientation and the faces of the first are coplanar to the supporting plane of the second (and vice versa).

Despite this refinement, some segments still cannot be used later during the polygonization process. These correspond to architectural details represented by a small number of faces due to the limited resolution of MVS meshes (see Fig. 4). Therefore, we assign to each planar segment an *importance* value equal to its *area* over the *surface area* of the *entire mesh*. With an *importance threshold*, we select only those segments which are meaningful to us and discard the rest.

Having established the set of primitives in the original model, we finally record their interrelationships in the structure graph. In this work, we focus only on *adjacency* relations between the primitives. Furthermore, we assume that two primitives are adjacent if they share at least one common vertex.

3.3. Polygonization

With the structure of the input model fully defined, we move to the polygonization itself. Our polygonization process is divided into three separate stages: **(1)** the construction of a *building scaffold*, **(2)** the generation of *candidate faces*, and **(3)** the selection of candidate faces through *optimization* to form the simplified model.

3.3.1. Building scaffold

Similar to Variational Shape Approximation (VSA) (Cohen-Steiner et al., 2004), our method also approximates the original model with a set of planar shapes *(proxies)*. Each of these proxies corresponds to a primitive we detected via segmentation. To form the simplified mesh, we first define the boundaries of these proxies. These boundaries should connect proxies whose primitives are also adjacent in the original model, thus preserving the adjacencies recorded in our structure graph.

Here, we determine the borders of the proxies with the construction of the *building scaffold*. This scaffold is a graph consisting of any *sharp features* detected in the original model. We specifically focus on sharp features of two types; *corners* (formed out of *three* adjacent primitives) and *non-planar edges* (formed out of *two* adjacent primitives). To detect corners, we identify all triplets of adjacent regions in the structure graph and compute the intersections of their supporting planes. In the same way, we compute the intersections for pairs of adjacent regions to detect non-planar edges (see Fig. 5).

3.3.2. Candidate faces

With the construction of the building scaffold, we first approximate the original mesh with a *wireframe mesh* consisting only of vertices and edges. We also define the faces of this mesh (*candidate faces*) through the following procedure:

- For each planar region, we collect its scaffold edges and project them on the supporting plane of that region.
- The projections of the edges form a *2D arrangement* (see Fig. 6), a subdivision of the plane into vertices, edges, and faces (Agarwal and Sharir, 2000). The faces of this arrangement define the candidate faces representing the planar region in our simplified mesh.

The outcome of this procedure is the formation of a *proxy mesh* (see Fig. 7). However, several adjacencies recorded in the structure graph might be incorrect due to segmentation errors, which results in candidate faces that do not correspond to any of the primitives from the input model. To reliably eliminate these redundant faces, the construction of the final, simplified mesh is achieved via an optimization process.

3.3.3. Optimization

We adopt and adapt here the optimization process developed by Nan et al. (Nan and Wonka, 2017) for the reconstruction of polygonal surfaces from point clouds. This optimization is based on the formulation of a *binary linear programming* problem (Papadimitriou and Steiglitz, 1982; Williams, 2009). For this type of problem, each of the unknowns is represented by a variable whose value can be either 0 (not chosen) or 1 (chosen). These variables are connected through (a) an energy function that maximizes the expectation of some reconstruction objectives and (b) a set of *constraints* that ensure the resulting mesh is both *manifold* and *watertight*. For the binary variable x_i of each candidate face, our objective function consists of three energy terms: *face coverage*, *data fitting*, and *model complexity*.

Face coverage. The face coverage term is related to the area of a candidate face covered by the faces of the original mesh (see Fig. 8),

$$E_c = \frac{1}{A(M)} \sum_{i=1}^{N} x_i \cdot (A(f_i) - A(M_i^a)) \tag{1}$$

where $A(M)$ is the total surface area of the simplified mesh M, $A(f_i)$ the area of the candidate face f_i, and $A(M_i^a)$ the face area covered by the original region. This term favours choosing faces with high coverage from the original mesh. Computing the $A(M)$ term is not possible as the area of the simplified mesh is unknown. However, we expect that the simplified version should conform to the original mesh. This allows us to use the surface area of its *bounding box* instead, i.e., $A(M) \approx A(bbox)$.

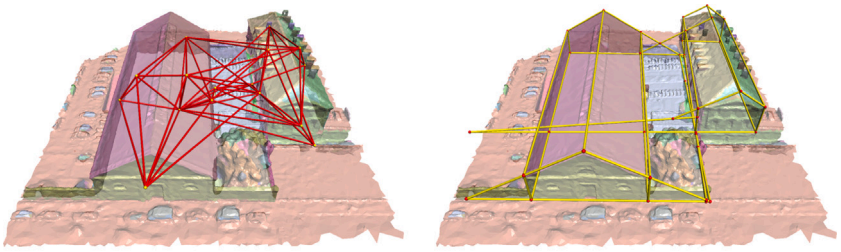

(a) Structure graph (b) Building scaffold

Fig. 5. By traversing the structure graph **(a)**, the adjacency of the planar segments can be recovered. Thus, the scaffold vertices and edges **(b)** are computed as the intersections of their supporting planes.

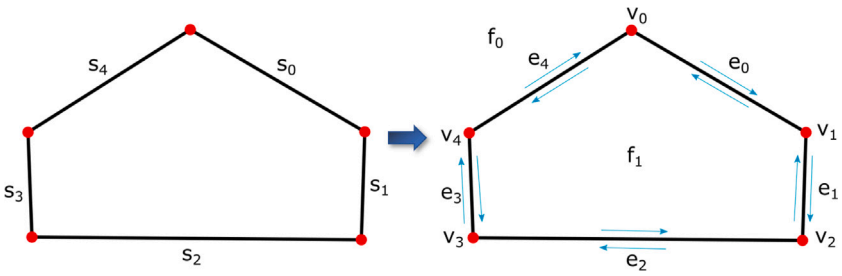

Fig. 6. A 2D arrangement of the projected scaffold edges.

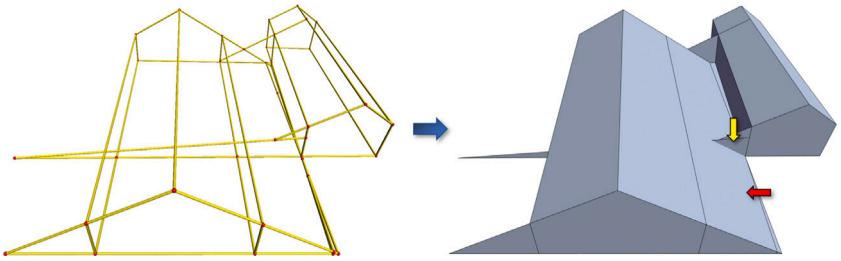

Fig. 7. Proxy mesh. The 2D arrangements of the scaffold edges (left) form a set of candidate faces (right) for the proxy mesh. Notice that errors in the structure graph may cause the production of additional faces (red arrow) or self-intersections (yellow arrow). (For interpretation of the references to colour in this figure legend, the reader is referred to the web version of this article.)

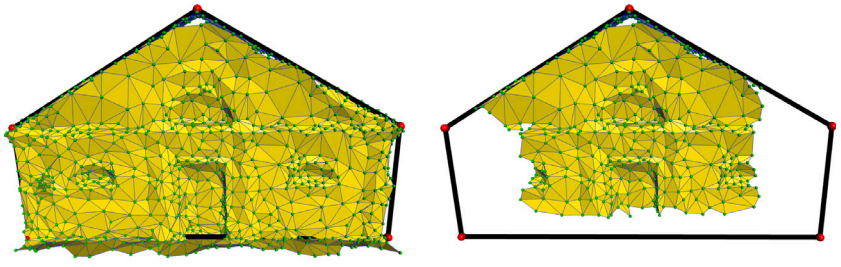

(a) 0.98 (b) 0.53

Fig. 8. Two examples of face coverage. The border of the candidate face are coloured in black, while the faces of the input mesh in yellow. The value below each figure indicates the coverage ratio of each face. (For interpretation of the references to colour in this figure legend, the reader is referred to the web version of this article.)

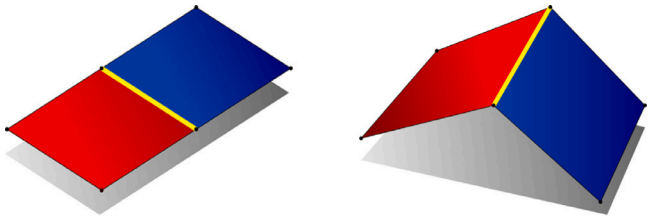

Fig. 9. **(a)** Planar and **(b)** non-planar edges. The latter are edge whose incident faces are not co-planar, and they are used to define distinct features in meshes.

Data fitting. Apart from the area coverage, we also consider the number of faces from the input mesh covering a candidate face. This is expressed through the *data fitting* term

$$E_f = 1 - \frac{1}{|F|}\sum_{i=1}^{N} x_i \cdot s(f_i), \tag{2}$$

where $|F|$ is the total number of the original faces and $s(f_i)$ the number of those faces covering the candidate face. As a consequence, faces with a great amount of supporting faces have a higher chance to be selected in the final solution.

Model complexity. The data-fitting term complies with discontinuities in the original mesh (such as holes). To avoid such gaps in the final model and enforce the creation of large planar regions, we introduce a *model complexity* term, related to the number of model *features* (details). These features are represented by *edges* which are incident to faces from different supporting planes (see Fig. 9). To this end, we define the model complexity term to evaluate the *ratio* of non-planar edges over the total number of edges in the simplified model

$$E_m = \frac{1}{|E|}\sum_{i=1}^{|E|} c(e_i), \tag{3}$$

where $|E|$ is the total number of edges in the proxy mesh. On the other hand, $c(e_i)$ is an indicator function, whose value is determined by the configuration of the candidate faces *adjacent* to an edge and *selected* in the final optimization solution. If the faces are co-planar, the function has a value of zero (Fig. 9(a)). Otherwise, if the faces are not co-planar forming a sharp edge, the function has a value of one (Fig. 9(b)).

We select the optimal subset of candidate faces to form the simplified model by *minimizing* the weighted sum of these energies. The complete objective function, along with the hard constraints to ensure that the resulting mesh is both *manifold* and *watertight* (meaning that each edge is adjacent to *exactly* two faces), is given in Eq. (4).

$$\min_{x} \lambda_f \cdot E_f + \lambda_c \cdot E_c + \lambda_m \cdot E_m$$
$$\text{s.t.} \begin{cases} \sum_{j \in N(e_i)} x_j = 2 \text{ or } 0, & 1 \le i \le |E| \\ x_i \in \{0,1\}, & 1 \le i \le N \end{cases} \tag{4}$$

This optimization is bound to produce a simplified, topologically valid representation, despite the various geometric or topological defects in the input MVS mesh (see Fig. 10).

3.4. Implementation details

We have implemented our method in C++ using the CGAL library. Through experimentation, we performed the computation of planarity for our segmentation technique over 3-ring neighbourhoods for both mesh vertices and faces. The distance threshold varied according to both the *minimum width* of a building component we wish to detect (see Fig. 11) and the respective scale of the input mesh. To eliminate architectural details from the simplification procedure, we used an importance threshold of 1% for all the available models. Finally, the weights of the energy terms in our optimization were those defined by Nan and Wonka (2017), i.e., $\lambda_f = 0.43$, $\lambda_c = 0.27$, and $\lambda_m = 0.30$.

4. Results & analysis

We applied our method over a set of building models. The results are shown in Fig. 12 where most of the examples refer to open meshes, with the exceptions of models **(d)** and **(g)**. Furthermore, we performed polygonization over individual building models, again with the exception of model **(a)** which contains two separate buildings. The available meshes consist only of planar components in various configurations, with roof superstructures varying from simple, flat roofs [**(h)**, **(i)**] to more complicated assemblies [**(e)**, **(f)**]. The level of noise in those models is also variable, from clean [**(d)**, **(g)**] to more distorted ones [**(h)**, **(i)**], and dependent on the noise of the original point clouds.

Although the result of our method is always a closed mesh, the input is still allowed to be open which is the case with most building models extracted from urban scenes. To complete the simplified model, our implementation exploits the ground plane of the original urban scene from which the input model was extracted. However, an alternative implementation could allow the user to import such a plane, according to their needs.

We assess the conformity of our simplified version to the original model by computing the *Hausdorff distance* between the two meshes (Guthe et al., 2005). From Table 1, we observe that the RMSE error is small for both closed and open meshes, which indicates that our simplified versions closely follow the initial building models, especially when the original mesh is clean [**(d)**, **(g)**]. Our simplification method performs rather well, also when the input model is quite noisy [**(h)**, **(i)**].

A comparison between model **(a)** and models **(b)**, **(c)** reveals that the method can be applied to an urban scene consisting of multiple buildings. Nevertheless, processing each building model individually results in much more detailed models of higher geometric accuracy. This is because the area of building primitives remains constant while their importance changes as the mesh surface area increases. This leads eventually to their exclusion from the simplification process.

Parameters. We have conducted a quantitative analysis of the effect of the parameters on the final results. This analysis shows that ring neighbourhoods of order 3 are more than sufficient for the detection of borders between adjacent planar regions (see Fig. 3). Any lower order is not sensitive enough for this task, while any higher order increases the computational time considerably.

The distance threshold is highly dependent on the scale of the input model. Nevertheless, our experiments have shown that the mean edge length of the input model is a good indicator of the distance threshold that achieves the best results for all the tested data.

Furthermore, the importance threshold of 1% is sufficient for the polygonization of all our tested models. Experimentation reveals that this parameter has a maximum range from 0.1% to 5%, in which it produces simplified meshes conforming adequately to the original structure (see Fig. 13).

As for the weights of the energy terms in the optimization process, a wide range of their values can produce the same results, except for cases where one of the data-fitting or coverage terms is extremely favoured over the other (in a proportion greater than four to one). A small coverage coefficient allows the selection of a larger amount of faces, while a high value of it reduces the candidate faces to only a few (see Fig. 14). In general, the data-fitting coefficient should always be slightly higher since coverage is a much stricter indicator of face validity, thus disregarding most of the candidate set.

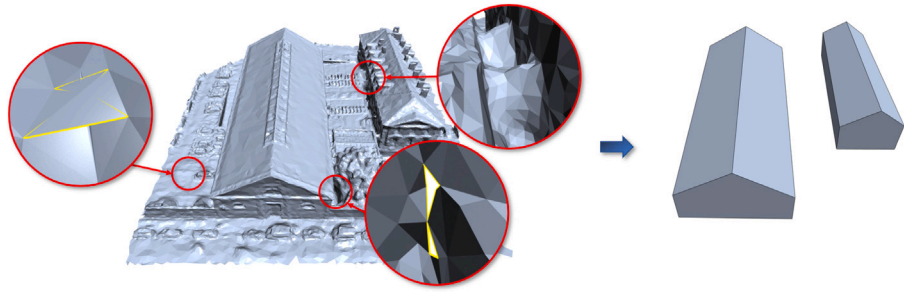

Fig. 10. Robustness. Even though various defects are present in the original mesh (holes, self-intersections, occlusions etc.), our proposed method is guaranteed to produce a simplified version of the original model.

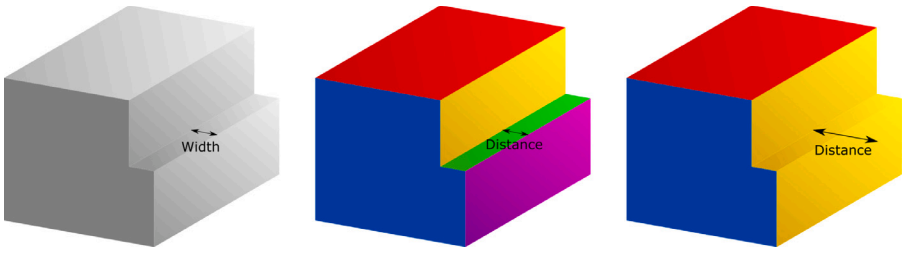

Fig. 11. By altering the distance threshold of our segmentation method, we are able to detect or ignore building components (here depicted with different colours).

Table 1
Statistics on the simplified meshes. Notice that for this comparison, the polygonal faces of the simplified meshes have been previously triangulated for the visualization purpose.

Mesh (Fig. 13)	(a)	(b)	(c)	(d)	(e)	(f)	(g)	(h)	(i)
# faces (original)	70,910	13,389	21,454	27,258	6,172	9,923	39,044	39,948	37,269
# faces (simplified)	32	46	110	338	62	38	284	130	100
Planarity (s)	0.9	0.3	0.4	0.5	0.1	0.2	0.7	0.8	0.7
Segmentation (s)	12.4	1.3	1.4	2.5	0.1	0.3	5.7	23.1	10.9
Struct. graph (s)	0.5	0.1	0.2	0.2	0.1	0.1	0.4	0.5	0.4
Simplification (s)	0.2	0.1	0.2	0.6	0.1	0.1	0.9	0.3	0.2
RMSE (% BBox Diagonal)	0.5	0.4	0.3	0.1	0.4	0.5	0.1	1.0	0.8

Structural accuracy. Certain inconsistencies might be observed between the original models and our simplified versions. These inconsistencies are related to parts of the structure that appear **(a)** with different geometry in each model or **(b)** only in one of the two models. The former error (see Fig. 15(a)) is associated with flaws due to segmentation, i.e., the detection of less planar components than the ones necessary to fully approximate a given model. The latter one (see Fig. 15(b)) with the hard constraints imposed in our optimization process to ensure the manifoldness of the final result. Specifically, the hard constraints will include candidate faces in the resulting model regardless of their face coverage, if the manifoldness of the final mesh remains unaffected.

Comparisons. Fig. 16 presents a comparison between our method and other available simplification and polygonization methods. In this comparison, we have simplified a model to have the same number of faces for each method. We observe that the error of our method is smaller than those from all the competing techniques. Additionally, the error on our results is distributed uniformly along the mesh surface contrary to the other methods where the error is located on specific model features. Furthermore, our approach is the only one to produce lightweight models, valid to be used for further applications, despite the topological and geometric defects of the original mesh.

We have also compared the performance of our method to the plane assembly technique PolyFit. We applied both methods to the building block model shown in Fig. 17 for the same number of initially detected planes. Our method took less than two seconds while PolyFit could not finish the optimization within two hours (see Table 2 for more details). This comparison proved that our approach is computationally more efficient than PolyFit.

Limitations.

Our definition of structure is based on the detection of the *building primitives*, along with their interrelationships, which, in our case, are limited only to adjacency relationships. This requires that both of these elements need to be recovered so that the model structure is completely acquired. This requirement may not be satisfied due to two reasons, both related to mesh segmentation (see Fig. 18):

(a) The set of building primitives is not fully recovered. This may occur when the distance threshold is too big or when the input mesh is “smooth”, meaning that the curvature on the borders of planar regions changes gradually. As a result, certain components cannot be represented with a planar region and therefore, are ignored during the construction of the building scaffold.
(b) The topological relationships, *necessary* to recover the border of a planar region in the building scaffold (as vertices and edges), are not included in the structure graph. This may occur when the region extends in a limited area of the mesh, i.e., it shares a common border with some of the adjacent regions, smaller than the one required to define a closed shape.

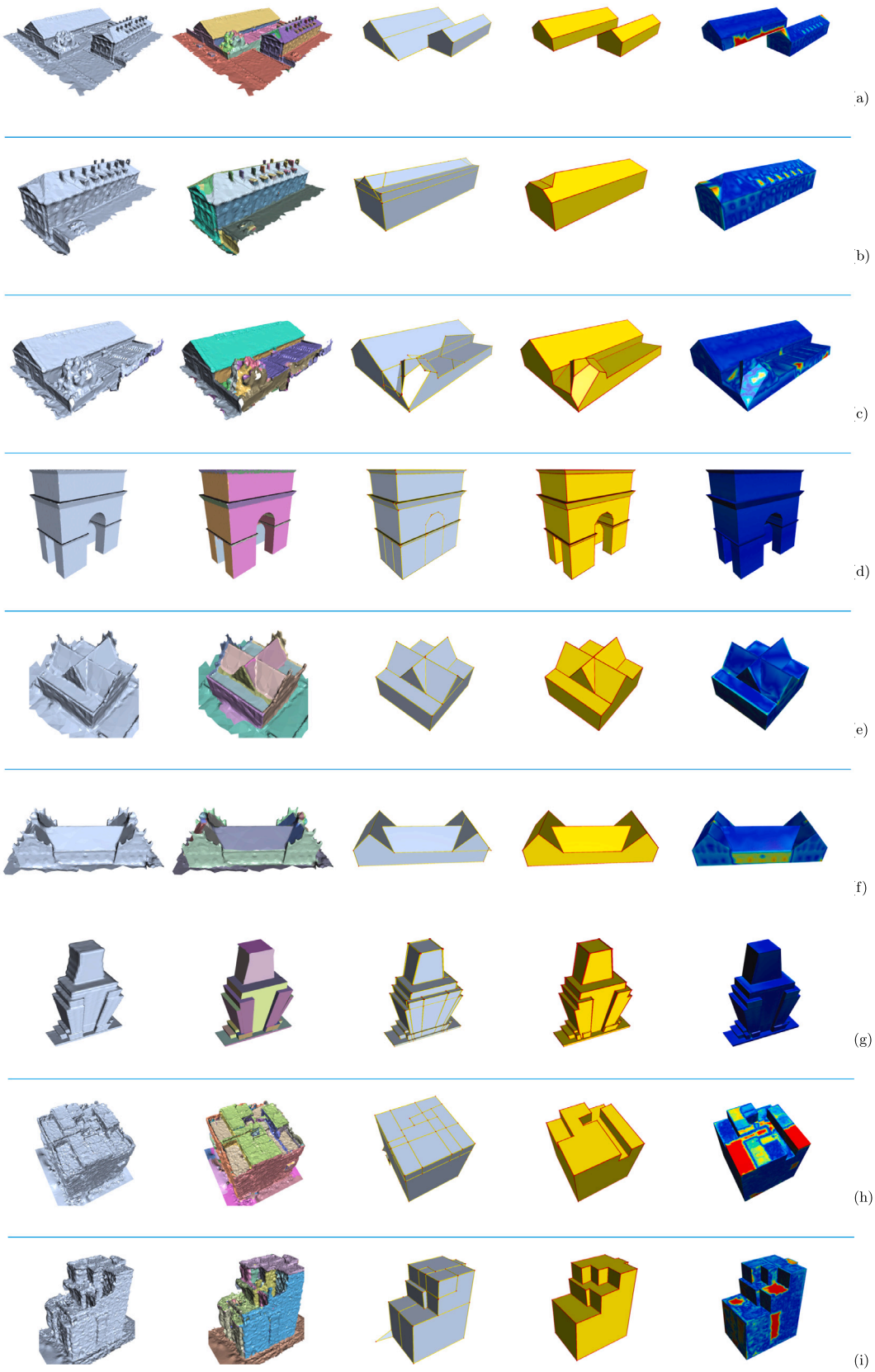

Fig. 12. Simplification results. From left to right: original model, refined segmentation, candidate faces, simplified mesh, and the visualization of the Hausdorff distance defined between the input model and the result.

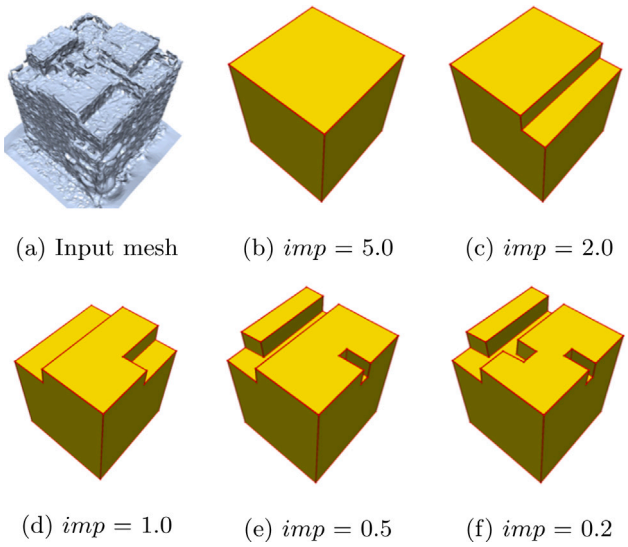

Fig. 13. The effect of the importance threshold.

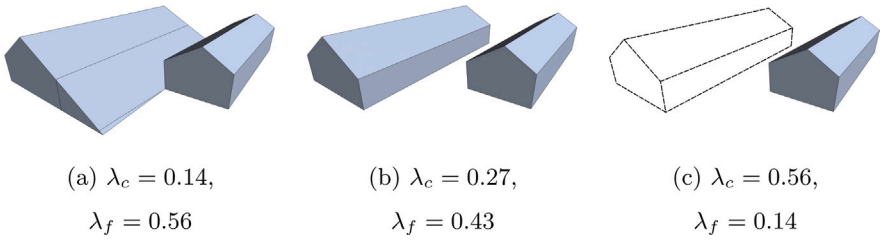

Fig. 14. The effect of the energy coefficients.

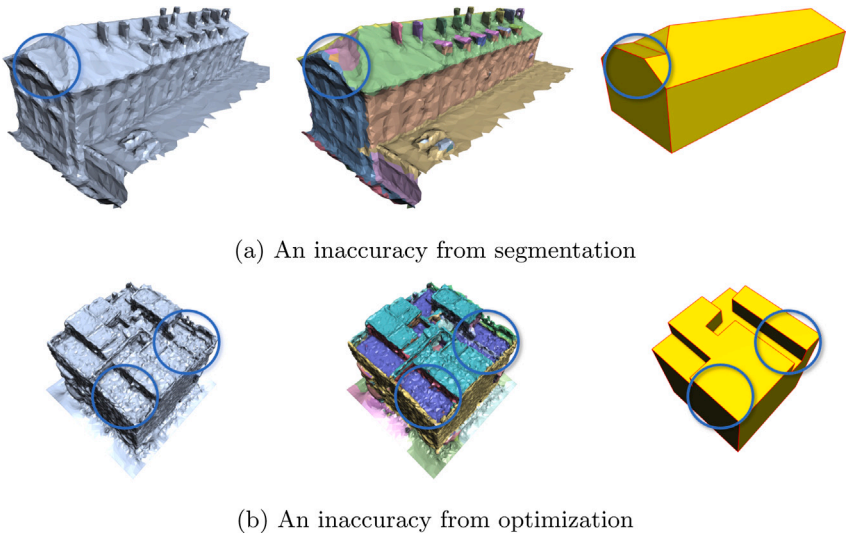

Fig. 15. Two types of structure inaccuracy.

Table 2
Comparison between our method and PolyFit. The execution of PolyFit was terminated after two hours.

	#planes	#candidate	#variables	#constraints	time
Ours	144	454	2100	804	1.7 s
PolyFit	144	43655	133701	278183	>2 h

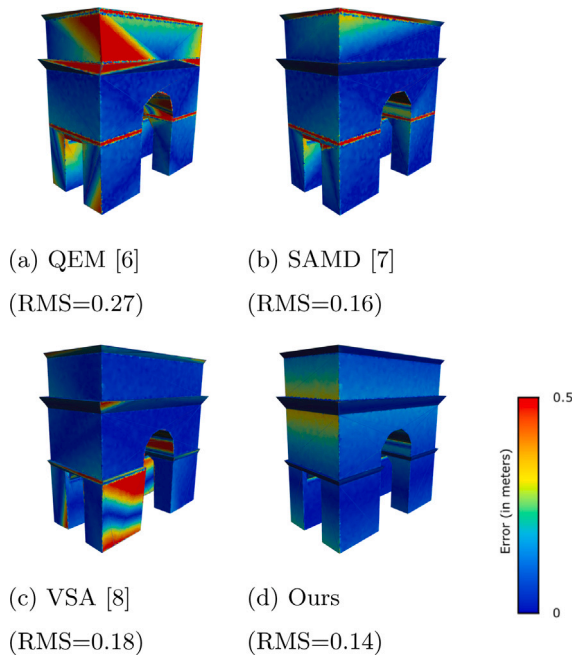

Fig. 16. Comparison between our method and other simplification techniques for the same number of faces.

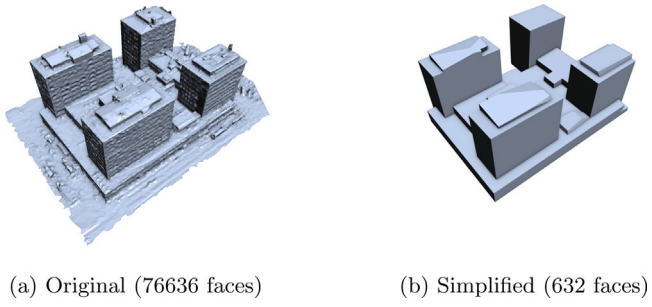

Fig. 17. Application of our method on a building block.

Another limitation of our method is that it is mostly developed for reconstructing individual buildings. If two buildings that are very close or adjacent, it is possible that the resulting volumes intersect, which would be due to elongated and/or unwanted features. Processing these two buildings together would be one way to avoid this (although these buildings could be merged into one instance).

It is also theoretically possible that, for one input model, two or more faces would intersect and be selected for the final model (see as an example the candidate faces where the yellow arrow points in Fig. 7). However, during our tests, we have never encountered such a case. This is because those faces get assigned a low confidence value before the optimization, and are therefore never selected (the data fitting term forbids choosing the ones with a low confidence value). In theory, this could be guaranteed if we detected self-intersections in the candidate set as part of an iterative process before the optimization. As soon as such a case is found, we could split the two corresponding faces into four new ones, and then the hard constraints (i.e., each edge is associated with 0 or 2 faces) would ensure the final model is free of self-intersections.

5. Conclusions

We have presented a novel approach for the structure-driven production of simple, topologically valid building models out of dense MVS meshes. Our *structure graph*, an abstraction of the structure of the original model, stands as the cornerstone of the simplification procedure. Its main role is to dictate the geometric operation necessary to reproduce simplified versions of the building primitives, as well as their initial configuration in the 3D space. As a consequence, our method is both accurate and computationally efficient. It should be noticed that currently regularity is not enforced in or after the simplification. This means that corners and edges in the resulting simplified model are not adjusted to feature orthogonality, and neither are the façades forced to be vertical. In other words, our method is generic. However, such a regularization step could be applied to our output as a post-processing step.

Applications. Our approach can be included as an individual part of a more general procedure for the reconstruction of entire urban scenes. Utilizing *semantic segmentation* (Landrieu and Simonovsky, 2018; Zhu et al., 2018), the buildings of a given urban scene can be isolated, simplified separately with our proposed technique and then, recombined with the rest of the scene (as shown in Fig. 1).

Future work. We would like to further refine our means for recovering the structure of the original model, thus improving its robustness. In addition to the planar primitives, we would like to incorporate additional primitive geometries (such as cylinders, spheres, and cones), to handle a wider range of building structures.

Declaration of competing interest

The authors declare that they have no known competing financial interests or personal relationships that could have appeared to influence the work reported in this paper.

Appendix

See Algorithm 1.

Algorithm 1 Region growing with k-ring planarity

Input:
- Triangle Surface Mesh $\mathcal{M}$ with faces F
- k-ring Planarity Estimates $\{p\}$
- k-ring Neighbouring Face Finding Function $\Omega_k(.)$
- Distance Threshold d^t

Output: Triangles assigned to segments
Initialize:
- Regions $\{R\} \leftarrow \emptyset$ // a list of integers (face indices)
- Available Faces $\{F\} \leftarrow \{1, 2,..., m\}$ // a list of integers (face integers)

while $\{V\} \neq \emptyset$ **do**
- Current Region: $\{R_c\} \leftarrow \emptyset$ // face indices
- Current Seeds: $\{S_c\} \leftarrow \emptyset$ // face indices
- Face with highest planarity $\{F\} \leftarrow f_{max}$
- $\{S_c\} \leftarrow \{S_c\} \cup f_{max}$
- $\{V\} \leftarrow \{V\} \setminus f_{max}$
- Find k-ring neighbouring faces $\{B_c\} \leftarrow \Omega_k\{f_{max}\}$
- Fit plane to Neighbours $plane \leftarrow \text{PCA}\{B_c\}$
- **while** $\{S_c\} \neq \emptyset$ **do**
  - $\{B_c\} \leftarrow \emptyset$ // face indices
  - **for** s in $\{S_c\}$ **do**
    - $\{B_c\} \leftarrow \{B_c\} \cup \Omega_1\{s\}$ // 1-ring neighbours
    - $\{S_c\} \leftarrow \{S_c\} \setminus s$
  - **end for**
  - **for** B in $\{B_c\}$ **do**
    - $\{v_B\} \leftarrow$ vertices of B
    - **if** $B \in \{F\}$ and $dist(B, plane) \leq d^t$ **then**
      - $\{R_c\} \leftarrow \{R_c\} \cup B$
      - $\{V\} \leftarrow \{V_c\} \setminus \{v_B\}$
      - $\{S_c\} \leftarrow \{S_c\} \setminus \{v_B\}$
    - **end if**
  - **end for**
  - Re-fit plane to current region $plane \leftarrow \text{PCA}\{R_c\}$
- **end while**
- Add current region $\{R\} \leftarrow \{R_c\}$

end while

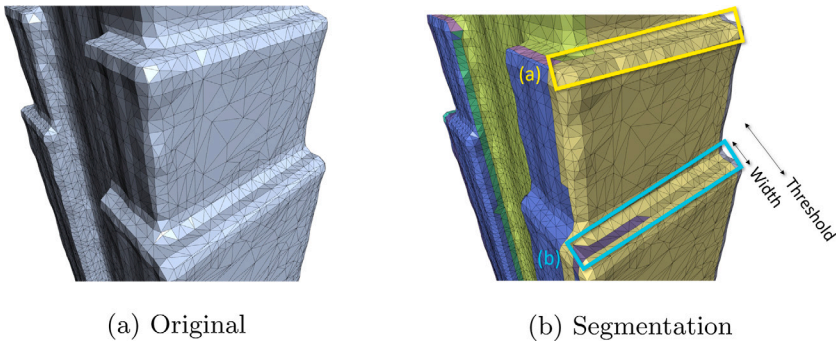

Fig. 18. Structure errors.

References

Agarwal, P.K., Sharir, M., 2000. Arrangements and their applications. In: Handbook of Computational Geometry. North-Holland, Amsterdam, pp. 49–119. http://dx.doi.org/10.1016/B978-044482537-7/50003-6, URL http://www.sciencedirect.com/science/article/pii/B9780444825377500036.

Bauchet, J.-P., 2019. Kinetic Data Structures for the Geometric Modeling of Urban Environments (Theses). Université Côte d'Azur, Inria, France, https://hal.inria.fr/tel-02432386.

Bernardini, F., Mittleman, J., Rushmeier, H.E., Silva, C.T., Taubin, G., 1999. The ball-pivoting algorithm for surface reconstruction. IEEE Trans. Vis. Comput. Graph. 5 (4), 349–359.

Biljecki, F., Stoter, J., Ledoux, H., Zlatanova, S., Çöltekin, A., 2015. Applications of 3D city models: State of the art review. ISPRS Int. J. Geo-Inf. 4 (4), 2842–2889. http://dx.doi.org/10.3390/ijgi4042842, http://www.mdpi.com/2220-9964/4/4/2842.

Bódis-Szomorú, A., Riemenschneider, H., Gool, L.J.V., 2015. Superpixel meshes for fast edge-preserving surface reconstruction. In: CVPR. IEEE Computer Society, pp. 2011–2020.

Chauve, A.-L., Labatut, P., Pons, J.-P., 2010. Robust piecewise-planar 3D reconstruction and completion from large-scale unstructured point data. In: 2010 IEEE Computer Society Conference on Computer Vision and Pattern Recognition. IEEE, http://dx.doi.org/10.1109/cvpr.2010.5539824.

Chen, J., Chen, B., 2007. Architectural modeling from sparsely scanned range data. Int. J. Comput. Vis. 78 (2–3), 223–236. http://dx.doi.org/10.1007/s11263-007-0105-5.

Cohen-Steiner, D., Alliez, P., Desbrun, M., 2004. Variational shape approximation. ACM Trans. Graph. 23 (3), 905–914. http://dx.doi.org/10.1145/1015706.1015817.

Fang, H., 2019. Geometric Modeling of Man-Made Objects at Different Level of Details (Ph.D. thesis).

Fang, H., Lafarge, F., Desbrun, M., 2018. Planar shape detection at structural scales. In: IEEE Conference on Computer Vision and Pattern Recognition (CVPR). Salt Lake City, United States, URL https://hal.inria.fr/hal-01741650.

Furukawa, Y., Hernández, C., 2015. Multi-view stereo: A tutorial. Found. Trends Comput. Graph. Vis. 9 (1–2), 1–148.

Garland, M., Heckbert, P.S., 1997. Surface simplification using quadric error metrics. In: Proceedings of the 24th Annual Conference on Computer Graphics and Interactive Techniques. SIGGRAPH '97, ACM Press/Addison-Wesley Publishing Co., New York, NY, USA, pp. 209–216. http://dx.doi.org/10.1145/258734.258849.

Gatzke, T., Grimm, C., 2006. Estimating curvature on triangular meshes. Int. J. Shape Model. 12, 1–28. http://dx.doi.org/10.1142/S0218654306000810.

Guthe, M., Borodin, P., Klein, R., 2005. Fast and accurate hausdorff distance calculation between meshes. J. WSCG 13 (2), 41–48, URL http://wscg.zcu.cz/wscg2005/Papers_2005/Journal/!WSCG2005_Journal_Final.pdf.

Holzmann, T., Oswald, M., Pollefeys, M., Fraundorfer, F., Bischof, H., 2017. Plane-based surface regularization for urban 3D reconstruction. In: 28th British Machine Vision Conference.

Jonsson, M., 2016. Make it Flat : Detection and Correction of Planar Regions in Triangle Meshes (Master's thesis). Linköping University, Computer Vision, p. 82.

Kazhdan, M.M., Bolitho, M., Hoppe, H., 2006. Poisson Surface reconstruction. In: Symposium on Geometry Processing. In: ACM International Conference Proceeding Series, vol. 256, Eurographics Association, pp. 61–70.

Kelly, T., Femiani, J., Wonka, P., Mitra, N.J., 2017. BigSUR: large-scale structured urban reconstruction. ACM Trans. Graph. 36 (6), 204:1–204:16.

Landrieu, L., Simonovsky, M., 2018. Large-scale point cloud semantic segmentation with superpoint graphs. In: Proceedings of the IEEE Conference on Computer Vision and Pattern Recognition, pp. 4558–4567.

Li, M., Nan, L., Smith, N., Wonka, P., 2016. Reconstructing building mass models from UAV images. Comput. Graph. 54, 84–93.

Mitra, N.J., Wand, M., Zhang, H.R., Cohen-Or, D., Kim, V.G., Huang, Q., 2013. Structure-aware shape processing. In: SIGGRAPH Asia 2013, Hong Kong, China, November 19-22, 2013, Courses. pp. 1:1–1:20. http://dx.doi.org/10.1145/2542266.2542267.

Monszpart, A., Mellado, N., Brostow, G.J., Mitra, N.J., 2015. Rapter. ACM Trans. Graph. 34 (4), 1–12. http://dx.doi.org/10.1145/2766995.

Nan, L., Wonka, P., 2017. PolyFit: Polygonal surface reconstruction from point clouds. In: ICCV. IEEE Computer Society, pp. 2372–2380.

Oesau, S., Lafarge, F., Alliez, P., 2015. Planar shape detection and regularization in tandem. Comput. Graph. Forum 35 (1), 203–215. http://dx.doi.org/10.1111/cgf.12720.

Papadimitriou, C., Steiglitz, K., 1982. Combinatorial optimization: Algorithms and complexity. IEEE Trans. Acoust. Speech Signal Process. 32, http://dx.doi.org/10.1109/TASSP.1984.1164450.

Pauly, M., Gross, M., Kobbelt, L.P., 2002. Efficient simplification of point-sampled surfaces. In: Proceedings of the Conference on Visualization '02. VIS '02, IEEE Computer Society, Washington, DC, USA, pp. 163–170, http://dl.acm.org/citation.cfm?id=602099.602123.

Rouhani, M., Lafarge, F., Alliez, P., 2017. Semantic segmentation of 3D textured meshes for urban scene analysis. ISPRS J. Photogramm. Remote Sens. 123, 124–139. http://dx.doi.org/10.1016/j.isprsjprs.2016.12.001.

Salinas, D., Lafarge, F., Alliez, P., 2015. Structure-aware mesh decimation. Comput. Graph. Forum 34 (6), 211–227. http://dx.doi.org/10.1111/cgf.12531.

Schnabel, R., Wahl, R., Klein, R., 2007. Efficient RANSAC for point-cloud shape detection. Comput. Graph. Forum 26 (2), 214–226.

Valentin, J.P., Sengupta, S., Warrell, J., Shahrokni, A., Torr, P.H., 2013. Mesh based semantic modelling for indoor and outdoor scenes. In: 2013 IEEE Conference on Computer Vision and Pattern Recognition. IEEE, http://dx.doi.org/10.1109/cvpr.2013.269.

Verdie, Y., Lafarge, F., Alliez, P., 2015. LOD Generation for urban scenes. ACM Trans. Graph. 34 (3), 30:1–30:14.

Wang, J., Fang, T., Su, Q., Zhu, S., Liu, J., Cai, S., Tai, C., Quan, L., 2016. Image-based building regularization using structural linear features. IEEE Trans. Vis. Comput. Graph. 22 (6), 1760–1772.

Williams, H., 2009. Logic and Integer Programming, vol. 130. http://dx.doi.org/10.1007/978-0-387-92280-5.

Zhu, L., Shen, S., Gao, X., Hu, Z., 2018. Large scale urban scene modeling from MVS meshes. In: ECCV (11). In: Lecture Notes in Computer Science, vol. 11215, Springer, pp. 640–655.